HHS Public Access

Author manuscript

Cancer Res. Author manuscript; available in PMC 2020 July 15.

Published in final edited form as:

Cancer Res. 2019 July 15; 79(14): 3662–3675. doi:10.1158/0008-5472.CAN-18-3464.

Pre-existing commensal dysbiosis is a host-intrinsic regulator of tissue inflammation and tumor cell dissemination in hormone receptor-positive breast cancer

Claire Buchta Rosean[1], **Raegan R. Bostic**[2], **Joshua C. M. Ferey**[3], **Tzu-Yu Feng**[1], **Francesca N. Azar**[1], **Kenneth S. Tung**[4], **Mikhail G. Dozmorov**[5], **Ekaterina Smirnova**[5], **Paula D. Bos**[6], **Melanie R. Rutkowski**[1]

[1]Department of Microbiology, Immunology, and Cancer Biology, University of Virginia, Charlottesville, VA 22903

[2]Department of Cell Biology, University of Virginia, Charlottesville, VA 22903

[3]University of Virginia School of Medicine, Charlottesville, VA 22903

[4]Department of Pathology, University of Virginia, Charlottesville, VA 22903

[5]Department of Biostatistics, Virginia Commonwealth University, Richmond, VA 23298

[6]Department of Pathology, Massey Cancer Center, Virginia Commonwealth University, Richmond, VA 23298

Abstract

It is unknown why some patients with hormone receptor-positive (HR^+) breast cancer present with more aggressive and invasive disease. Metastatic dissemination occurs early in disease and is facilitated by crosstalk between the tumor and tissue environment, suggesting that undefined host-intrinsic factors enhance early dissemination and the probability of developing metastatic disease. Here, we have identified commensal dysbiosis as a host-intrinsic factor associated with metastatic dissemination. Using a mouse model of HR^+ mammary cancer, we demonstrate that a pre-established disruption of commensal homeostasis results in enhanced circulating tumor cells and subsequent dissemination to the tumor-draining lymph nodes and lungs. Commensal dysbiosis promoted early inflammation within the mammary gland that was sustained during HR^+ mammary tumor progression. Furthermore, dysbiosis enhanced fibrosis and collagen deposition both systemically and locally within the tumor microenvironment and induced significant myeloid infiltration into the mammary gland and breast tumor. These effects were recapitulated both by directly targeting gut microbes using non-absorbable antibiotics and by fecal microbiota transplantation of dysbiotic cecal contents, demonstrating the direct impact of gut dysbiosis on mammary tumor dissemination. This study identifies dysbiosis as a pre-existing, host-intrinsic regulator of tissue inflammation, myeloid recruitment, fibrosis, and dissemination of tumor cells in HR^+ breast cancer.

Corresponding author: Melanie R. Rutkowski; MR6 G526, 345 Crispell Dr, Charlottesville, VA 22908. 434-297-8103. mr2ee@virginia.edu.

Conflict of interest disclosure statement: The authors declare no potential conflicts of interest.

Keywords

commensal dysbiosis; inflammation; myeloid recruitment; fibrosis; hormone receptor-positive breast cancer

INTRODUCTION

Breast cancer is a major global health issue, with 1 in 8 women expected to be diagnosed with breast cancer in their lifetime. The majority of breast cancers (~65%) are diagnosed as hormone receptor-positive (HR^+; estrogen- and progesterone-receptor$^+$, $HER2^{neg/low}$) (1). Due to the effectiveness of adjuvant hormonal therapies, HR^+ breast cancer has a more favorable short-term prognosis compared with more aggressive subtypes such as triple-negative breast cancer (TNBC) (2). However, patients diagnosed with HR^+ breast cancer have heterogeneity in tumor aggressiveness and overall survival, with a subset of patients remaining at significant risk for developing recurrent disease after 5 years of standard endocrine therapy (3). This heterogeneity in outcome results in a small but sustained risk for developing recurrent metastatic disease 5 years or more after initial remission (4).

Metastatic dissemination to distal lymph nodes and the lungs occurs early in HR^+ breast cancer progression (5). Although it remains unknown whether host-intrinsic differences in immune function contribute to increased early dissemination of tumor cells, lymph node involvement is one of the most reliable predictors of recurrent disease (6,7) and identifies patients that would benefit from extended adjuvant hormonal therapy. This therapy reduces late recurrence for some high-risk patients but also commonly results in undesirable and potentially serious side effects (8). Identification of early or pre-existing host-associated factors that influence the evolution of disseminated breast cancer could therefore aid in the development of alternative interventions for patients that are at highest risk for recurrent metastatic disease.

Factors such as obesity, genetic polymorphisms, race, diet, and chronic use of antibiotics have been associated with adverse outcomes in breast cancer (9–12). All of these factors are also linked to a disruption in the homeostasis of the commensal microbiome. The commensal microbiota is a host-intrinsic regulator of systemic innate and adaptive immune function (13–15). Altered diversity in the microbiota, known as dysbiosis, can influence the systemic immune environment (16) and lead to increased production of inflammatory mediators that associate with a poor outcome for multiple diseases, including cancer (17–19). Indeed, infection of $APC^{Min/+}$ mice with *H. hepaticus* led to increased inflammation and significant incidence of breast cancer in female mice (20), supporting the idea that perturbation of commensal organisms can influence breast cancer risk (21). However, it is currently unknown whether pre-existing commensal dysbiosis leads to changes within the tissue and/or tumor microenvironment that promote tumor aggressiveness and metastatic dissemination.

We set out to determine if commensal microbes influence breast cancer progression: specifically, if pre-existing dysbiosis in the commensal microbiome associates with poor outcomes in HR^+ breast cancer. Here, we demonstrate that a disruption in commensal

homeostasis promotes tumor cell dissemination to distal sites, enhances fibrosis and collagen deposition both systemically and locally within the tissue and tumor microenvironment, and results in significant early inflammation and myeloid infiltration into the mammary tissue and tumor. These effects are initiated by signals from the gut, as commensal dysbiosis induced both by treatment with non-absorbable antibiotics and by fecal microbiota transplantation (FMT) of dysbiotic cecal contents recapitulates these outcomes. This study identifies commensal dysbiosis as a host-intrinsic regulator of tissue inflammation, myeloid recruitment, fibrosis, and dissemination of tumor cells – all of which contribute to reduced survival in HR^+ breast cancer.

MATERIALS AND METHODS

Mice

5–8-week-old female C57BL/6 mice were purchased from Charles River Laboratories (Wilmington, MA). L-Stop-L-*KRas*^{G12D}*p53*$^{flx/flx}$L-Stop-L-*Myristoylated p110α*−GFP^+ mice on a C57BL/6 background (22) were bred and maintained in house. All animals were maintained in pathogen-free barrier facilities at the University of Virginia. All experiments in this study were approved by the University of Virginia Institutional Animal Care and Use Committee.

Genetic tumor model and cell lines

The poorly metastatic HR^+ mouse mammary cancer cell line BRPKp110 has been described previously (23). 5E5 BRPKp110 cells were injected orthotopically into the abdominal mammary fat pad. The highly metastatic mouse mammary cancer cell line PyMT, which expresses luciferase, was cloned from a metastatic tumor derived from the HR^+ MMTV-PyMT model as previously described (24). In experiments using this cell line, 1E5 PyMT cells were injected orthotopically into the abdominal mammary fat pad. Cell lines were authenticated by maintaining at less than four passages, monitoring of morphology, and testing for mycoplasma. Autochthonous mammary tumors were induced in L-Stop-L-*KRas*^{G12D}*p53*$^{flx/flx}$L-Stop-L-*Myristoylated p110α*−GFP^+ mice on a C57BL/6 background as previously described (22). Briefly, tumors were initiated via intraductal injection of 2.5E7 PFU of adenovirus-Cre through the nipple in the fourth mammary fat pad.

Antibiotic treatment

For most experiments, mice were orally gavaged for 14 days with antibiotic cocktail or water as a vehicle control as previously described (25). After 14 days of gavage, mice were left untreated for four days before tumor initiation to allow for the establishment of commensal dysbiosis. Mice treated with an absorbable (systemic) antibiotic cocktail received 100μl of a cocktail containing vancomycin (0.5 mg/ml), ampicillin (1 mg/ml) metronidazole (1 mg/ml), neomycin (1 mg/ml), and gentamicin (1 mg/ml). Vehicle-treated mice received 100μl of water as a control. Mice treated with non-absorbable (non-systemic) antibiotics received 200μl of a cocktail containing neomycin (2 mg/ml) and bacitracin (2 mg/ml). Vehicle-treated mice received 200μl of water as a control. All antibiotics were purchased from Sigma-Aldrich (St. Louis, MO) with the exception of vancomycin (Gold Biotechnology; St. Louis, MO). For FMT experiments, dysbiosis was induced in donor mice

as described above. Cecal contents from dysbiotic and non-dysbiotic animals were collected, homogenized, and frozen at −80C in sterile 1:1 glycerol/PBS. Recipient mice were orally gavaged with absorbable antibiotics for 7 days, followed by 3 consecutive days of oral gavage with either dysbiotic or non-dysbiotic cecal contents. After the final day of gavage, recipient mice were rested for 7 days before tumor initiation to allow for microbial engraftment.

Flow cytometry

Tumors, mammary glands, and lungs were removed, weighed, homogenized (gentleMACS Dissociator, Miltenyi Biotec, Germany), and digested with collagenase D (Sigma-Aldrich) for 30 minutes at 37C prior to 70μm filtration. Tumor-draining lymph nodes were homogenized using glass slides and processed as the other tissues. Flow cytometry was performed by staining single-cell suspensions with Zombie Aqua viability dye (Biolegend, San Diego, CA), blocking Fc receptors with anti-CD16/32 (93, purified), and staining with anti-mouse antibodies at the manufacturer's recommended dilution. Myeloid cell infiltration was quantitated in tumors and normal-adjacent mammary glands by surface staining with anti-mouse CD45 (30-F11, Pacific Blue), CD11b (M1/70, PE/Cy7), F4/80 (BM8, PerCP/Cy5.5), CD86 (GL-1, BV650), CD206 (C068C2, PE/Dazzle-594), Ly6C (HK1.4, APC/Cy7), and Ly6G (1A8, FITC) and intracellular staining using anti-mouse arginase-1 (IC5868P, PE) and IL-6 (MP5–20F3, APC). Tumor cell dissemination was quantitated using single-cell suspensions from lungs and tumor-draining lymph nodes through surface staining with anti-mouse CD45 (30-F11, PE) and intracellular staining with anti-GFP (FM264G, APC). Circulating tumor cells from the blood were quantitated as previously described (26). Briefly, equal volumes of EDTA-treated blood underwent red blood cell lysis, were plated into 6-well culture dishes, and incubated for 7 days. Cells were detached and stained as described for quantitation of disseminated tumor cells. All antibodies were purchased from Biolegend with the exception of anti-arginase-1 (R&D Systems; Minneapolis, MN). Counting beads (AccuCount, Spherotech; Lake Forest, IL) were added to samples at the manufacturer's recommended concentration, and the samples were subsequently run on a Beckman Coulter CytoFLEX cytometer (Brea, CA) and analyzed using FlowJo (Ashland, OR).

Cytokine analysis

Cytokines and chemokines were analyzed in serum and mammary glands using a custom multiplex U-PLEX assay from Meso Scale Diagnostics (Rockville, MD). Blood was collected by cardiac puncture and allowed to clot at room temperature for 30 minutes before centrifugation and collection of serum. Mammary glands were flash frozen in liquid nitrogen, ground in a mortar and pestle with lysis buffer (150mM NaCl, 20mM Tris, 1mM EDTA, 1mM EGTA, 1% Triton X-100, pH 7.5), sonicated, and centrifuged. The supernatants were then collected, protein concentrations were quantified by BCA assay (Pierce, Thermo Fisher Scientific), and supernatants were used for U-PLEX analysis. Mammary gland readouts were normalized to total protein input.

Histology and microscopy

To quantitate fibrosis, tissues were fixed in neutral-buffered formalin, paraffin-embedded, and cut in 5μm sections (Research Histology Core, University of Virginia). Slides were stained using PicroSirius Red (0.1% Direct Red 80 in saturated aqueous picric acid, Sigma-Aldrich). Fibrosis was quantified using Image J software by calculating the area of tissue and the intensity of red staining. To examine mammary gland pathology, hematoxylin and eosin-stained slides were scored by a pathologist in a blinded fashion. To determine estrus cycling, vaginal lavages were collected daily after the 14-day antibiotic gavage period and examined for vaginal cytology. Mice were considered to be cycling when they progressed from proestrus to estrus.

Bioluminescent imaging

Mice were injected intravenously with 3 mg of D-luciferin potassium salt (Gold Biotechnology) and allowed to saturate systemically for 2 minutes. Mice were then euthanized, and lungs were removed for ex vivo imaging to detect bioluminescent light emission using a Caliper IVIS Spectrum bioluminescence instrument (PerkinElmer, Waltham, MA; Molecular Imaging Core, University of Virginia). Bioluminescence from ex vivo lungs was calculated as photons per second within a standardized region of interest and normalized to final tumor burden.

16S microbiome sequencing

Sequencing was performed by the University of Maryland Institute for Genome Science.

*S*equences were demultiplexed using the mapping file split_libraries_fastq.py, a QIIME-dependent script. Fastq files were split by using seqtk (https://github.com/lh3/seqtk), primer sequences removed using TagCleaner (0.16), followed by downstream processing using DADA2 Workflow for Big Data and dada2 (v. 1.5.2) (https://benjjneb.github.io/dada2/bigdata.html). Forward and reverse reads were trimmed using lengths of 255 and 225 bp, respectively, to contain no ambiguous bases, have a minimum quality score of 2, and contain less than two expected errors based on quality score. Reads were assembled and chimeras removed per dada2 protocol.

Taxonomic assignments—Taxonomy was assigned to each amplicon sequence variant (ASV) generated by dada2 using a combination of the SILVA v128 database and the RDP naïve Bayesian classifier as implemented in the dada2 R package species level assignments. Read counts for ASVs assigned to the same taxonomy were summed for each sample.

Statistical Analysis—Alpha diversity of microbiome samples was measured using Shannon alpha diversity measure and a Kruskal-Wallis test to measure significance. Beta diversity of microbiome sequences was assessed using Bray-Curtis dissimilarity measures based upon relative abundance data and a Permanova test was performed to measure statistical significance.

Metabolomic analysis

Metabolomic analysis was performed by Metabolon, Inc. (Morrisville, NC). Principal component analysis was performed using the "prcomp()" R function (https://www.R-project.org/). Samples were colored according to tumor status, dysbiosis, or both (sample annotations). The association between the sample annotations and the first two principal components was tested by one-way ANOVA. A significant association suggests that the variability explained by a principal component is driven by a corresponding sample annotation. Calculations and visualizations were performed in the R/Bioconductor environment v.3.5.1.

Statistical analysis

P values were generated using Student's t-tests (unpaired, two-tailed, at 95% confidence interval) or ANOVA when appropriate. Statistical significance is designated when $p < 0.05$.

RESULTS

Pre-established commensal dysbiosis results in enhanced tumor cell dissemination.

To evaluate the impact of commensal dysbiosis on metastatic HR^+ breast cancer, we used the poorly-metastatic GFP^+ BRPKp110 syngeneic model (23) of HR^+ mammary cancer. Our goal was to determine whether preexisting commensal dysbiosis affects mammary tumor metastasis and progression. To that end, mice were orally gavaged with a broad-spectrum cocktail of antibiotics (25) for 14 days, a sufficient duration to enable outgrowth of antibiotic-resistant commensal species (27). Mice were then rested for four days following cessation of antibiotics to allow for dysbiotic reacquisition of commensal species (28), and mammary tumors were initiated by injecting tumor cells into the fourth abdominal mammary fat pad (Figure 1A).

Bacterial composition was evaluated in the feces of mice on the day of tumor initiation using 16S rDNA sequencing. Compared to vehicle-treated mice, those receiving antibiotics showed shifts in bacterial communities at both the phylum and genus levels (Figure S1A). Using a Bray-Curtis dissimilarity measure, beta diversity between the two treatment groups differed significantly (Figure S1B). Antibiotic-treated mice had a significant reduction in community richness within the gut, as indicated by calculation of Shannon alpha diversity index (Figure S1C), as well as enlarged ceca (Figure S1D), demonstrating that antibiotic-treated mice had commensal dysbiosis prior to tumor initiation.

To evaluate the impact of antibiotic-driven gut dysbiosis in the breast tissue, we first performed histological examination of the mammary gland at the time of tumor implantation. Blinded histopathological scoring of the mammary tissues indicated that the antibiotic treatment resulted in minimal changes to tissue morphology (Figure S2A–B).

Metabolic output often reflects the status of the commensal ecosystem. In order to indirectly evaluate whether functional changes to the commensal ecosystem within the mammary tissue microenvironment occur in response to antibiotic treatment or tumor status, we compared metabolites in normal-adjacent mammary tissue from antibiotic- or non-antibiotic

treated mice, with or without a tumor 6 days after tumor cell inoculation. As a positive control, we collected feces from treated and non-treated mice. Similar to changes observed with 16S rDNA sequencing at day 0, global fecal metabolites significantly differed when compared by dysbiotic status, but were independent of tumor status (Figure S2C). On the contrary, metabolites within the mammary tissue remained unchanged despite dysbiosis or tumor status (Figure S2D). Thus, at the time of tumor implantation, histological and metabolic changes within the mammary tissue were similar between treatment groups. Together, these data suggest that the mammary tissue is minimally affected by antibiotic treatment.

Using the poorly-metastatic syngeneic BRPKp110 model, we evaluated tumor cell dissemination to lungs and axillary lymph nodes by flow cytometric quantitation of GFP $^{+}$CD45^{-} mammary tumor cells (Figure S3A). Significantly more disseminated tumor cells were detected within the lungs (Figure 1B and 1C), peripheral blood (Figure 1D, Figure S3B), and tumor-draining axillary lymph nodes (Figure 1E, Figure S3C) of dysbiotic mice. Importantly, although commensal bacteria have been shown to modulate estrogen levels, which could impact the estrus cycle and tumor growth kinetics of HR^{+} mammary tumors, we did not observe differences in primary tumor growth kinetics in mice with or without commensal dysbiosis (Figure 1F). Estrus cycle monitoring between the last day of antibiotic treatment until the day of tumor implantation using vaginal lavage confirmed no substantial differences in cycle patterns (Figure S4A) or in the proportions of animals that were cycling, as defined by progressing from proestrus to estrus (Figure S4B). These data suggest that commensal dysbiosis influences tumor cell seeding to distal sites, independent of changes to the tissue microenvironment or estrus cycle.

We next evaluated whether pre-established commensal dysbiosis would impact tumor growth or metastatic dissemination in a more aggressive and metastatic tumor model. For these experiments, we used a tumor cell line that was derived from an advanced primary mammary tumor arising in the autochthonous MMTV-PyMT mouse model (24). Similar to what we observed using the BRPKp110 model, we found significantly greater dissemination of tumors into the lungs, independent of tumor volume (Figure 1G–H), and tumors progressed with equal kinetics regardless of the dysbiotic status of the animals (Figure 1I). Together, these results suggest that commensal dysbiosis has a sustained impact on the dissemination of HR^{+} mammary cancer, and that increased dissemination in mice with commensal dysbiosis is occurring independently of tumor growth kinetics.

We also tested the effects of commensal dysbiosis using a GFP^{+} inducible autochthonous model (22) that is established by targeting latent mutations with intraductal delivery of adenovirus-Cre. Using a similar experimental approach as depicted in Figure 1A, despite variable tumor kinetics, no significant differences in primary tumor growth between dysbiotic and non-dysbiotic groups were observed (Figure S5A). However, this variability makes it challenging to evaluate effects on tumor cell dissemination. To confirm if dysbiosis-driven, host-intrinsic differences induce dissemination in the autochthonous model, we performed paired tumor transfers into dysbiotic or non-dysbiotic recipient mice. Autochthonous mammary tumors were induced in wild-type mice without commensal dysbiosis, sterilely excised when they reached approximately 1cm in diameter, and equal-

weight fragments from the same tumor section were surgically implanted in the mammary tissue of recipient animals pretreated with antibiotics or vehicle gavage as described in Figure 1A. After the implanted tumors grew to an advanced size, lungs and axillary lymph nodes from the recipient mice were examined for the presence of disseminated tumor cells. Similar to what we observed using the syngeneic models, lungs from dysbiotic mice showed significantly greater frequencies of disseminated tumor cells (Figure S5B–C) whereas there was a non-significant increase in GFP^+ tumor cells in distal lymph nodes (Figure S5D). Together, these results confirm that commensal dysbiosis enhances tumor cell dissemination independently of primary tumor growth, and suggest that host-associated changes in response to commensal dysbiosis, not tumor-intrinsic differences in invasive capacity, enhance tumor dissemination.

Commensal dysbiosis leads to enhanced inflammation and myeloid cell infiltration within the mammary gland.

To identify possible microenvironmental factors associated with increased dissemination in tumor-bearing mice with commensal dysbiosis, we first defined the immunological changes occurring within the primary tumor microenvironment, specifically within the mammary tissue. Previous studies have demonstrated that inflammation within the mammary tissue associates with an increased risk for breast cancer (29). However, it is not well understood how this inflammation arises. The commensal microbiome is important for the maintenance of systemic and local immune homeostasis, giving rise to the possibility that commensal dysbiosis may result in a disruption of mammary tissue homeostasis and increased inflammation within the tissue. To examine the effects of commensal dysbiosis on the mammary gland during tumor progression, mammary tissues were harvested during early (day 12) and advanced (day 27) stages of tumor progression (Figure 2A). Mammary glands from non-tumor-bearing mice with or without dysbiosis were also evaluated in parallel. To normalize the systemic effects of hormones on mammary gland homeostasis and immune function, estrus cycles were synchronized in all animals prior to analysis using a modified Whitten effect (30).

Macrophages within the mammary gland associate with an increased risk of developing metastatic breast cancer (31). We therefore determined whether commensal dysbiosis influenced the frequencies and numbers of macrophages during early or advanced stages of mammary tumor progression. During early stages of tumor progression, the presence of a tumor was sufficient to significantly enhance myeloid accumulation into the normal-adjacent mammary gland (Figure 2B). This effect persisted into advanced stages of tumor progression, resulting in a substantial increase in myeloid frequencies within the normal-adjacent mammary gland (Figure 2C). However, commensal dysbiosis lead to a dramatic and significant increase in total accumulated myeloid cells within the normal-adjacent mammary glands at both early (Figure 2B) and advanced (Figure 2C) stages of tumor progression. Because tumors progressed with similar kinetics, these results suggest that commensal dysbiosis synergizes with a developing tumor to enhance myeloid cell infiltration within mammary tissue. Importantly, these data indicate that the effects of pre-established commensal dysbiosis on myeloid-driven inflammation within the mammary gland are sustained throughout tumor progression. Similar to published studies in humans

(31), myeloid cells infiltrating into normal-adjacent mammary tissue in dysbiotic mice expressed high levels of the inflammatory mediators arginase-1 and IL-6, specifically in the context of an early developing mammary tumor (Figure 2D). However, during advanced stages of tumor progression, myeloid production of arginase-1 and IL-6 was unchanged (Figure 2E). These results demonstrate that commensal dysbiosis promotes the early recruitment of inflammatory myeloid cells into the mammary tissue microenvironment.

We next wanted to define signals that arise in response to commensal dysbiosis and could enhance the recruitment of inflammatory myeloid cells into the breast tissue. Therefore, mammary tissues were harvested prior to tumor initiation (pre-tumor; day 0) and during early (early tumor; day 12) stages of tumor progression. Similar to the experiment depicted in Figure 2A, estrus cycles were synchronized prior to each experimental endpoint (Figure 2F). We focused our analysis on three myeloid chemoattractants that also associate with adverse outcomes in breast cancer: CXCL10 (32,33), CCL2 (34–36), and CXLC2 (37).

Compared with non-dysbiotic mice, commensal dysbiosis resulted in a significant upregulation of both CXCL10 and CCL2 within mammary tissue prior to tumor initiation (pre-tumor mammary tissue; day 0), while CXCL2 was elevated but not significantly different (Figure 2G). These data demonstrate that the systemic and/or local response to commensal dysbiosis culminates, at the very least, in low-level non-pathological inflammation within the mammary gland. Although the mammary gland inflammation eventually subsided in non-tumor-bearing dysbiotic mice, CXCL10, CCL2, and CXCL2 remained significantly elevated within normal-adjacent mammary glands in tumor-bearing mice with pre-established dysbiosis when compared to all other experimental groups (Figure 2G). Together, these data demonstrate that pre-existing commensal dysbiosis results in inflammation within the mammary gland that persists in the presence of a tumor during early stages of mammary tumor progression. Additionally, these data suggest that crosstalk occurring between an inflamed tissue and a developing tumor amplifies the accumulation of myeloid cells into the microenvironment, and that the effects of this crosstalk are likely sustained throughout early and advanced stages of tumor progression.

Dysbiosis induces early and sustained systemic inflammation and enhances myeloid infiltration into tumors.

In addition to promoting local inflammation within breast tissue, commensal dysbiosis also enhanced systemic inflammation. To examine the systemic impact of commensal dysbiosis, serum was collected prior to tumor initiation (pre-tumor serum; day 0) and at early (early tumor serum; day 12) and advanced (advanced tumor serum; day 27) stages of tumor progression. Serum was analyzed for the presence of GM-CSF, CCL2, and CXLC2, chemokines involved in myeloid cell generation and migration; and IL-22 and IL-23, cytokines that mediate inflammatory responses and that are associated with gut barrier function. We focused upon these two cytokines as expression of both IL-22 and IL-23 are enhanced in the serum of breast cancer patients and have been associated with tumor progression and decreased overall survival (38,39).

Interestingly, in response to commensal dysbiosis, all cytokines and chemokines tested were significantly increased in the serum of mice with established commensal dysbiosis prior to

tumor initiation. While no significant differences were observed in serum from dysbiotic or non-dysbiotic mice with or without early-stage mammary tumors, dysbiotic mice bearing advanced mammary tumors showed significantly increased serum CCL2 and a low but significant increase of IL-23, while levels of GM-CSF, CXCL2, and IL-22 were elevated but not significantly different (Figure 3A). Importantly, because tumors progress at similar rates regardless of dysbiotic status, enhanced serum cytokines were not due to differences in primary tumor burden.

Macrophages are one of the most abundant cell types within the breast tumor-microenvironment (40) and are a significant prognostic indicator of reduced survival for patients diagnosed with HR^+ breast cancer (41). Confirming this, the majority of myeloid infiltrates within the mammary tumor microenvironment at early and advanced stages of tumor progression were M2-like macrophages, based upon CD206 expression (Figure 3B). Similar to what we observed in normal-adjacent mammary glands, pre-established commensal dysbiosis resulted in enhanced total myeloid cell accumulation within both early and advanced mammary tumors. Importantly, advanced tumors from dysbiotic mice had significantly increased numbers of infiltrating tumor-promoting M2-like macrophages as compared with non-dysbiotic controls with equal tumor burden. Together, these data demonstrate that the systemic expression of inflammatory mediators is increased in dysbiotic tumor-bearing mice, enhancing myeloid recruitment into mammary tumors.

Dysbiosis enhances both local and systemic fibrosis in mammary tumor-bearing animals.

Enhanced stromal density, or dense breasts, is a well-established risk factor for developing metastatic breast cancer (42) and tumor-promoting inflammation in the breast (43). To determine whether commensal dysbiosis enhanced fibrosis within the tissue or tumor microenvironment or at systemic sites of metastatic dissemination, we stained tissues from dysbiotic and non-dysbiotic mice with PicroSirius Red to visualize collagen deposition. We found that pre-established commensal dysbiosis resulted in significant enhancement of collagen deposition within the normal-adjacent mammary gland (Figure 4A) and tumors (Figure 4B) of advanced tumor-bearing mice. We also observed a slight, but significant, increase in collagen accumulation within the lungs of advanced tumor-bearing dysbiotic mice (Figure 4C). Together, these data demonstrate that enhanced fibrosis at both local and distal sites are a long-term consequence of commensal dysbiosis during mammary cancer.

Dysbiotic phenotype is recapitulated using non-absorbable antibiotics.

The mammary gland is considered a mucosal surface with mammary-specific commensal microorganisms. Although significant metabolic changes within the mammary tissue of dysbiotic or non-dysbiotic mice were not observed (Figure S2C), suggestive of low to minimal impact on the commensal population residing within the mammary gland, the systemic effects of the antibiotic cocktail could theoretically contribute to enhanced tumor dissemination. Metronidazole is highly absorbed from the gut, whereas ampicillin has moderate systemic bioavailability after oral administration. To determine whether tumor dissemination and tissue inflammation arise due to a direct effect of antibiotics upon the tissue microflora or due to distal changes within the gut, commensal dysbiosis was induced using antibiotics that have no to minimal systemic bioavailability (44,45). This non-

absorbable antibiotic cocktail consisting of bacitracin and neomycin is well-established to specifically deplete bacteria within the gut (46).

Commensal dysbiosis initiated using non-absorbable antibiotics recapitulated the changes within the tissue and tumor microenvironments similar to what was observed using absorbable antibiotics. Myeloid cells infiltrating into normal-adjacent mammary glands of dysbiotic mice produced IL-6 or arginase-1 when commensal dysbiosis was established using absorbable or non-absorbable antibiotics (Figure 5A–B). Early myeloid cell recruitment into both mammary glands (Figure 5C) and mammary tumors (Figure 5D) was also enhanced in dysbiotic mice using both absorbable and non-absorbable antibiotics. During advanced tumor progression, fibrosis was enhanced both in mammary tumors (Figure 6A–B) and normal-adjacent mammary glands (Figure 6C–D) from dysbiotic mice using both absorbable and non-absorbable antibiotics.

Importantly, pre-established dysbiosis using non-absorbable antibiotics resulted in significant dissemination of tumor cells both into the peripheral blood (Figure 6E, Figure S6A) and to the lungs (Figure 6F, Figure S6B), similar to what was observed in animals treated with absorbable antibiotics. Although it cannot be ruled out that non-absorbable antibiotics indirectly affect the tissue commensal microorganisms or enhance bacterial translocation from the gut to distal sites such as the mammary tissue, these data demonstrate that targeted disruption of the gut microbiome is sufficient to initiate enhanced metastatic dissemination during breast cancer.

Fecal transfer of a dysbiotic microbiome enhances inflammation, myeloid cell infiltration, fibrosis, and tumor cell dissemination.

To determine whether a dysbiotic microbiome is sufficient to enhance mammary tumor cell dissemination, an FMT approach was used. Cecal contents from dysbiotic and non-dysbiotic donor mice were collected after 14 days of antibiotic gavage followed by a four-day rest, to recapitulate a dysbiotic microbiome at the time of tumor initiation. Cecal contents were transferred over 3 consecutive days into antibiotic-sterilized recipient SPF mice. BRPKp110 mammary tumors were initiated 7 days following FMT gavage (Figure 7A).

FMT of a dysbiotic or non-dysbiotic microbiome did not impact tumor kinetics (Figure S7A). Mice receiving FMT of dysbiotic cecal contents mirrored the phenotype of dysbiotic mice that had received extended gavage of absorbable or non-absorbable antibiotics. Specifically, mice receiving dysbiotic FMT showed enhanced infiltration of inflammatory myeloid cells into early mammary tissue (Figure 7B–7D) and increased myeloid cell accumulation into tumors (Figure 7E). Similar effects were observed during advanced stages of tumor progression, both within the mammary tissue (Figure 7F) and advanced tumors (Figure 7G). Mammary tissue (Figure 7H) and tumors (Figure 7I) from mice receiving dysbiotic FMT also showed enhanced tissue fibrosis. Importantly, mice receiving dysbiotic FMT, but not ‘normal’ FMT, had significantly enhanced tumor cell dissemination into the peripheral blood (Figure 7J, Figure S7B), within the lungs (Figure 7K, Figure S7C), and to the distal axillary lymph nodes (Figure 7L, Figure S7D). These data demonstrate that a dysbiotic microbiome, but not a normal microbiome, is sufficient to enhance metastatic dissemination during mammary cancer.

DISCUSSION

Our study demonstrates that commensal dysbiosis occurring prior to mammary cancer initiation is a host-intrinsic factor that contributes to increased tumor cell dissemination and metastatic seeding, leading to adverse outcomes. Our data support the idea that inflammation within the normal tissue microenvironment, in this case driven by a systemic response to commensal dysbiosis, precedes the development of aggressive breast cancer. In our model of HR^+ mammary cancer, although primary tumor growth remained unchanged, mice with pre-established commensal dysbiosis showed significantly enhanced tumor cell dissemination to the peripheral blood, lungs, and distal lymph nodes. These seemingly paradoxical data suggest that host factors associated with the growth of HR^+ tumors are distinct from those which contribute to metastatic dissemination. More investigation into myeloid function and tumor immune surveillance are necessary to understand these differences.

To understand the role of dysbiosis in driving metastatic dissemination, several key factors known to be involved in promoting metastasis and adverse outcome in HR^+ breast cancer were evaluated. The syngeneic model of commensal dysbiosis used in this study recapitulates features of breast cancer that have been independently associated with adverse outcome: enhanced inflammation both systemically and within the tissue environment; increased macrophage infiltration within tumors and normal-adjacent mammary tissue; and enhanced fibrosis within mammary tissue, tumors, and lungs. Importantly, enhanced dissemination as a result of commensal dysbiosis was observed regardless of the metastatic potential of the HR^+ mammary tumor models used in this study. Therefore, our data demonstrate that a disruption in commensal homeostasis results in the establishment of a tissue and/or tumor microenvironment that favors enhanced metastatic dissemination.

During commensal dysbiosis, chemokines involved in myeloid cell chemotaxis and recruitment were enhanced both systemically in serum and within the mammary tissue microenvironment of both tumor- and non-tumor-bearing dysbiotic mice. Whereas inflammation eventually resolved in dysbiotic non-tumor-bearing animals, the presence of a tumor in dysbiotic mice resulted in a persistent elevation of myeloid chemoattractants within the tissue microenvironment. Thus, it is likely that crosstalk occurs between the tumor and tissue microenvironments, leading to sustained inflammation and possible myeloid recruitment into these tissues in mice with commensal dysbiosis. Indeed, significantly more myeloid cells – particularly M2-like macrophages – infiltrated into mammary tumors and normal-adjacent mammary glands during early and advanced stages of tumor progression. Macrophages are one of the most abundant cell types within the breast tumor microenvironment. In patients, increased frequencies of macrophages within stroma and tumors associate with significantly reduced survival in HR^+ breast cancer (47). Macrophages increase angiogenesis, evasion of anti-tumor immunity, and promote metastatic dissemination and seeding of cells into distal sites. Thus, the accumulation of M2 macrophages likely plays a direct role in dysbiosis-dependent enhancement of tumor cell dissemination.

Inflammation within the mammary gland also increases susceptibility to developing breast cancer, as women with benign breast disease who later develop breast cancer have significantly greater proportions of inflammatory macrophages present within the tissue compared with women who do not go on to develop cancer (21,31). Similar to these human studies, in our model of HR^+ mammary cancer, significantly higher numbers of inflammatory macrophages producing IL-6 or arginase-1 were observed within normal-adjacent mammary tissue of mice with commensal dysbiosis during early stages of tumor development. Non-absorbable antibiotics that specifically target gut commensals and FMT of dysbiotic cecal contents also increased macrophage infiltration and inflammation within the mammary gland. Together, our studies demonstrate that commensal dysbiosis leads to a disruption in immune homeostasis and increased inflammation within both tumor- and non-tumor-associated tissue.

Supporting the idea that commensal dysbiosis contributes to the evolution of a more aggressive and high-grade disease, the induction of commensal dysbiosis using either absorbable or non-absorbable antibiotics or FMT of dysbiotic cecal contents resulted in significant fibrosis within both tumors and the tissue microenvironment. Collagen accumulation and stiffening within the extracellular matrix of tumors and within the tumor microenvironment is associated with increased dissemination of tumor cells into distal lymph nodes and lungs (48). These results suggest that a disruption of the gut microflora, not mammary tissue flora, prior to tumor initiation is sufficient to facilitate collagen accumulation within the tissue and tumor microenvironments. Furthermore, these data suggest that in HR^+ breast cancer, commensal dysbiosis leads to systemic changes that correspond with more invasive disease.

Factors that influence the development of dysbiosis are increasing worldwide, including rates of obesity and antibiotic use, highlighting the importance of elucidating the mechanisms by which commensal dysbiosis may promote cancer development and progression. While other studies have examined the impact of commensal microorganisms and/or dysbiosis in response to cancer treatments (49,50), this study is the first, to our knowledge, to directly assess whether commensal dysbiosis that is present at the time of tumor initiation impacts tumor aggressiveness and dissemination. Future studies will investigate the relationship between commensal microbe composition and fibrosis and myeloid cell invasion within pre-malignant mammary tissue. Additionally, it will be important to evaluate whether commensal dysbiosis during triple negative or $HER2^+$ breast cancer results in similar outcomes. Overall, our study identifies commensal dysbiosis as a pre-existing, host-intrinsic factor that promotes adverse outcomes in HR^+ breast cancer. Based upon this study, we speculate that commensal dysbiosis could thus serve as a potential biomarker or as a therapeutic target to reduce tumor-promoting inflammation within the tissue microenvironment.

Supplementary Material

Refer to Web version on PubMed Central for supplementary material.

ACKNOWLEDGMENTS

This study was supported by a Susan G Komen Career Catalyst award CCR17483602 (M. R. Rutkowski), IRG-17–097-31 (ACS, M.R. Rutkowski), the University of Virginia Cancer Center and support from NCI Cancer Center Support grant P30CA44570 as startup funds for M. R. Rutkowski, and training grant 5T32AI007496–24 (C. Buchta Rosean). The authors would like to acknowledge the University of Virginia Research Histology, Advanced Microscopy, Biorepository and Tissue Research Facility, Molecular Imaging, and Biomolecular Analysis Core Facilities, as well as the Carter Immunology Center. Additionally, we would like to thank Jose R. Conejo-Garcia for the BRPKp110 HR^+ breast tumor cell line and Steven N. Fiering for the L-Stop-L-*KRas*^{G12D}*p53*$^{flx/flx}$L-Stop-L-*Myristoylated p110α*−GFP^+ mice.

Financial support: Susan G Komen CCR17483602

REFERENCES

1. Burstein HJ, Cirrincione CT, Barry WT, Chew HK, Tolaney SM, Lake DE, et al. Endocrine therapy with or without inhibition of epidermal growth factor receptor and human epidermal growth factor receptor 2: a randomized, double-blind, placebo-controlled phase III trial of fulvestrant with or without lapatinib for postmenopausal women with hormone receptor-positive advanced breast cancer-CALGB 40302 (Alliance). J Clin Oncol 2014;32:3959–66. 10.1200/JCO.2014.56.7941. Epub 2014 Oct 27. [PubMed: 25348000]
2. DeSantis CE, Ma J, Goding Sauer A, Newman LA, Jemal A. Breast cancer statistics, 2017, racial disparity in mortality by state. CA Cancer J Clin 2017;67:439–48. 10.3322/caac.21412. Epub 2017 Oct 3. [PubMed: 28972651]
3. Song F, Zhang J, Li S, Wu J, Jin T, Qin J, et al. ER-positive breast cancer patients with more than three positive nodes or grade 3 tumors are at high risk of late recurrence after 5-year adjuvant endocrine therapy. Onco Targets Ther 2017;10:4859–4867.:10.2147/OTT.S142698. eCollection 2017. [PubMed: 29042797]
4. Colzani E, Johansson AL, Liljegren A, Foukakis T, Clements M, Adolfsson J, et al. Time-dependent risk of developing distant metastasis in breast cancer patients according to treatment, age and tumour characteristics. Br J Cancer 2014;110:1378–84 [PubMed: 24434426]
5. Hosseini H, Obradovic MM, Hoffmann M, Harper KL, Sosa MS, Werner-Klein M, et al. Early dissemination seeds metastasis in breast cancer. Nature 2016
6. Lee ES, Han W, Kim MK, Kim J, Yoo TK, Lee MH, et al. Factors associated with late recurrence after completion of 5-year adjuvant tamoxifen in estrogen receptor positive breast cancer. BMC Cancer 2016;16:430 [PubMed: 27388210]
7. Yamashita H, Ogiya A, Shien T, Horimoto Y, Masuda N, Inao T, et al. Clinicopathological factors predicting early and late distant recurrence in estrogen receptor-positive, HER2-negative breast cancer. Breast Cancer 2016;23:830–43 [PubMed: 26467036]
8. Davies C, Pan H, Godwin J, Gray R, Arriagada R, Raina V, et al. Long-term effects of continuing adjuvant tamoxifen to 10 years versus stopping at 5 years after diagnosis of oestrogen receptor-positive breast cancer: ATLAS, a randomised trial. Lancet 2013;381:805–16 [PubMed: 23219286]
9. Martin AM, Weber BL. Genetic and hormonal risk factors in breast cancer. J Natl Cancer Inst 2000;92:1126–35 [PubMed: 10904085]
10. Rutkowski MR, Stephen TL, Svoronos N, Allegrezza MJ, Tesone AJ, Perales-Puchalt A, et al. Microbially driven TLR5-dependent signaling governs distal malignant progression through tumor-promoting inflammation. Cancer Cell 2015;27:27–40 [PubMed: 25533336]
11. Nechuta S, Chen WY, Cai H, Poole EM, Kwan ML, Flatt SW, et al. A pooled analysis of post-diagnosis lifestyle factors in association with late estrogen-receptor-positive breast cancer prognosis. Int J Cancer 2016;138:2088–97 [PubMed: 26606746]
12. Ewertz M, Jensen MB, Gunnarsdottir KA, Hojris I, Jakobsen EH, Nielsen D, et al. Effect of obesity on prognosis after early-stage breast cancer. J Clin Oncol 2011;29:25–31 [PubMed: 21115856]
13. Abt MC, Osborne LC, Monticelli LA, Doering TA, Alenghat T, Sonnenberg GF, et al. Commensal bacteria calibrate the activation threshold of innate antiviral immunity. Immunity 2012;37:158–70 [PubMed: 22705104]

14. Clarke T, Davis K, Lysenko E, Zhou A, Yu Y, Weiser J. Recognition of peptidoglycan from the microbiota by Nod1 enhances systemic innate immunity. Nature medicine 2010;16:228–31
15. Schirmer M, Smeekens SP, Vlamakis H, Jaeger M, Oosting M, Franzosa EA, et al. Linking the Human Gut Microbiome to Inflammatory Cytokine Production Capacity. Cell 2016;167:1125–1930850304 [PubMed: 27814509]
16. Buchta Rosean CM, Rutkowski MR. The influence of the commensal microbiota on distal tumor-promoting inflammation. Seminars in immunology 2017
17. Willing BP, Russell SL, Finlay BB. Shifting the balance: antibiotic effects on host–microbiota mutualism. Nature Reviews Microbiology 2011;9:233–43 [PubMed: 21358670]
18. Kim Y-GG, Udayanga KG, Totsuka N, Weinberg JB, Núñez G, Shibuya A. Gut dysbiosis promotes M2 macrophage polarization and allergic airway inflammation via fungi-induced PGE_2. Cell host & microbe 2014;15:95–102 [PubMed: 24439901]
19. Arendt LM, McCready J, Keller PJ, Baker DD, Naber SP, Seewaldt V, et al. Obesity promotes breast cancer by CCL2-mediated macrophage recruitment and angiogenesis. Cancer Res 2013;73:6080–93 [PubMed: 23959857]
20. Rao VP, Poutahidis T, Ge Z, Nambiar PR, Boussahmain C, Wang YY, et al. Innate immune inflammatory response against enteric bacteria Helicobacter hepaticus induces mammary adenocarcinoma in mice. Cancer Res 2006;66:7395–400 [PubMed: 16885333]
21. Rao VP, Poutahidis T, Fox JG, Erdman SE. Breast cancer: should gastrointestinal bacteria be on our radar screen? Cancer Res 2007;67:847–50 [PubMed: 17283110]
22. Sheen MR, Marotti JD, Allegrezza MJ, Rutkowski M, Conejo-Garcia JR, Fiering S. Constitutively activated PI3K accelerates tumor initiation and modifies histopathology of breast cancer. Oncogenesis 2016;5
23. Allegrezza MJ, Rutkowski MR, Stephen TL, Svoronos N, Perales-Puchalt A, Nguyen JM, et al. Trametinib Drives T-cell-Dependent Control of KRAS-Mutated Tumors by Inhibiting Pathological Myelopoiesis. Cancer Res 2016;76:6253–65 [PubMed: 27803104]
24. Bos PD, Plitas G, Rudra D, Lee SY, Rudensky AY. Transient regulatory T cell ablation deters oncogene-driven breast cancer and enhances radiotherapy. J Exp Med 2013;210:2435–66 [PubMed: 24127486]
25. Hill DA, Hoffmann C, Abt MC, Du Y, Kobuley D, Kirn TJ, et al. Metagenomic analyses reveal antibiotic-induced temporal and spatial changes in intestinal microbiota with associated alterations in immune cell homeostasis. Mucosal immunology 2010;3:148–58 [PubMed: 19940845]
26. Harney AS, Arwert EN, Entenberg D, Wang Y, Guo P, Qian B-Z, et al. Real-time imaging reveals local, transient vascular permeability, and tumor cell intravasation stimulated by TIE2hi macrophage–derived VEGFA. Cancer discovery 2015
27. Becattini S, Taur Y, Pamer EG. Antibiotic-Induced Changes in the Intestinal Microbiota and Disease. Trends Mol Med 2016;22:458–78 [PubMed: 27178527]
28. Croswell A, Amir E, Teggatz P, Barman M, Salzman NH. Prolonged impact of antibiotics on intestinal microbial ecology and susceptibility to enteric Salmonella infection. Infect Immun 2009;77:2741–53. 10.1128/IAI.00006-09. Epub 2009 Apr 20. [PubMed: 19380465]
29. Iyengar NM, Zhou XK, Gucalp A, Morris PG, Howe LR, Giri DD, et al. Systemic Correlates of White Adipose Tissue Inflammation in Early-Stage Breast Cancer. Clin Cancer Res 2016;22:2283–9 [PubMed: 26712688]
30. Dalal SJ, Estep JS, Valentin-Bon IE, Jerse AE. Standardization of the Whitten Effect to induce susceptibility to Neisseria gonorrhoeae in female mice. Contemp Top Lab Anim Sci 2001;40:13–7. [PubMed: 11300681]
31. Degnim AC, Hoskin TL, Arshad M, Frost MH, Winham SJ, Brahmbhatt R, et al. Alterations in the Immune Cell Composition in Premalignant Breast Tissue that Precede Breast Cancer Development. Clinical cancer research : an official journal of the American Association for Cancer Research 2017
32. Jafarzadeh A, Fooladseresht H, Nemati M, Assadollahi Z, Sheikhi A, Ghaderi A. Higher circulating levels of chemokine CXCL10 in patients with breast cancer: Evaluation of the influences of tumor stage and chemokine gene polymorphism. Cancer Biomark 2016;16:545–54. 10.3233/CBM-160596. [PubMed: 27002757]

33. Ejaeidi AA, Craft BS, Puneky LV, Lewis RE, Cruse JM. Hormone receptor-independent CXCL10 production is associated with the regulation of cellular factors linked to breast cancer progression and metastasis. Exp Mol Pathol 2015;99:163–72. 10.1016/j.yexmp.2015.06.002. Epub Jun 14. [PubMed: 26079660]
34. Kitamura T, Qian BZ, Soong D, Cassetta L, Noy R, Sugano G, et al. CCL2-induced chemokine cascade promotes breast cancer metastasis by enhancing retention of metastasis-associated macrophages. J Exp Med 2015;212:1043–59 [PubMed: 26056232]
35. Ueno T, Toi M, Saji H, Muta M, Bando H, Kuroi K, et al. Significance of macrophage chemoattractant protein-1 in macrophage recruitment, angiogenesis, and survival in human breast cancer. Clin Cancer Res 2000;6:3282–9. [PubMed: 10955814]
36. Qian B-Z, Li J, Zhang H, Kitamura T, Zhang J, Campion LR, et al. CCL2 recruits inflammatory monocytes to facilitate breast-tumour metastasis. Nature 2011;475:222–5 [PubMed: 21654748]
37. Sharma B, Nawandar DM, Nannuru KC, Varney ML, Singh RK. Targeting CXCR2 enhances chemotherapeutic response, inhibits mammary tumor growth, angiogenesis, and lung metastasis. Mol Cancer Ther 2013;12:799–808 [PubMed: 23468530]
38. Rui J, Chunming Z, Binbin G, Na S, Shengxi W, Wei S. IL-22 promotes the progression of breast cancer through regulating HOXB-AS5. Oncotarget 2017;8:103601–12 [PubMed: 29262587]
39. Sheng S, Zhang J, Ai J, Hao X, Luan R. Aberrant expression of IL-23/IL-23R in patients with breast cancer and its clinical significance. Mol Med Rep 2018;17:4639–44 [PubMed: 29328397]
40. Williams CB, Yeh ES, Soloff AC. Tumor-associated macrophages: unwitting accomplices in breast cancer malignancy. NPJ breast cancer 2016;2
41. Gwak JM, Jang MH, Kim DI, Seo AN, one P-SY. Prognostic value of tumor-associated macrophages according to histologic locations and hormone receptor status in breast cancer. PloS one 2015
42. Boyd NF, Guo H, Martin LJ, Sun L, Stone J, Fishell E, et al. Mammographic density and the risk and detection of breast cancer. N Engl J Med 2007;356:227–36. 10.1056/NEJMoa062790. [PubMed: 17229950]
43. Huo CW, Hill P, Chew G, Neeson PJ, Halse H, Williams ED, et al. High mammographic density in women is associated with protumor inflammation. Breast Cancer Res 2018;20:92 10.1186/s13058-018-1010-2. [PubMed: 30092832]
44. Donoso J, Craig GO, Baldwin RS. The distribution and excretion of zinc bacitracin-14C in rats and swine. Toxicol Appl Pharmacol 1970;17:366–74 [PubMed: 5471557]
45. Pedersoli WM, Ravis WR, Jackson J, Shaikh B. Disposition and bioavailability of neomycin in Holstein calves. J Vet Pharmacol Ther 1994;17:5–11 [PubMed: 8196095]
46. Aguilera M, Cerdà-Cuéllar M, Martínez V. Antibiotic-induced dysbiosis alters host-bacterial interactions and leads to colonic sensory and motor changes in mice. Gut Microbes 2015;6:10–23 [PubMed: 25531553]
47. Gwak JM, Jang MH, Kim DI, Seo AN, Park SY. Prognostic value of tumor-associated macrophages according to histologic locations and hormone receptor status in breast cancer. PLoS One 2015;10:e0125728 10.1371/journal.pone.. eCollection 2015. [PubMed: 25884955]
48. Cox TR, Erler JT. Molecular Pathways: Connecting Fibrosis and Solid Tumor Metastasis. Clinical Cancer Research 2014;20
49. Vetizou M, Pitt JM, Daillere R, Lepage P, Waldschmitt N, Flament C, et al. Anticancer immunotherapy by CTLA-4 blockade relies on the gut microbiota. Science 2015;350:1079–84 [PubMed: 26541610]
50. Iida N, Dzutsev A, Stewart CA, Smith L, Bouladoux N, Weingarten RA, et al. Commensal bacteria control cancer response to therapy by modulating the tumor microenvironment. Science 2013;342:967–70 [PubMed: 24264989]

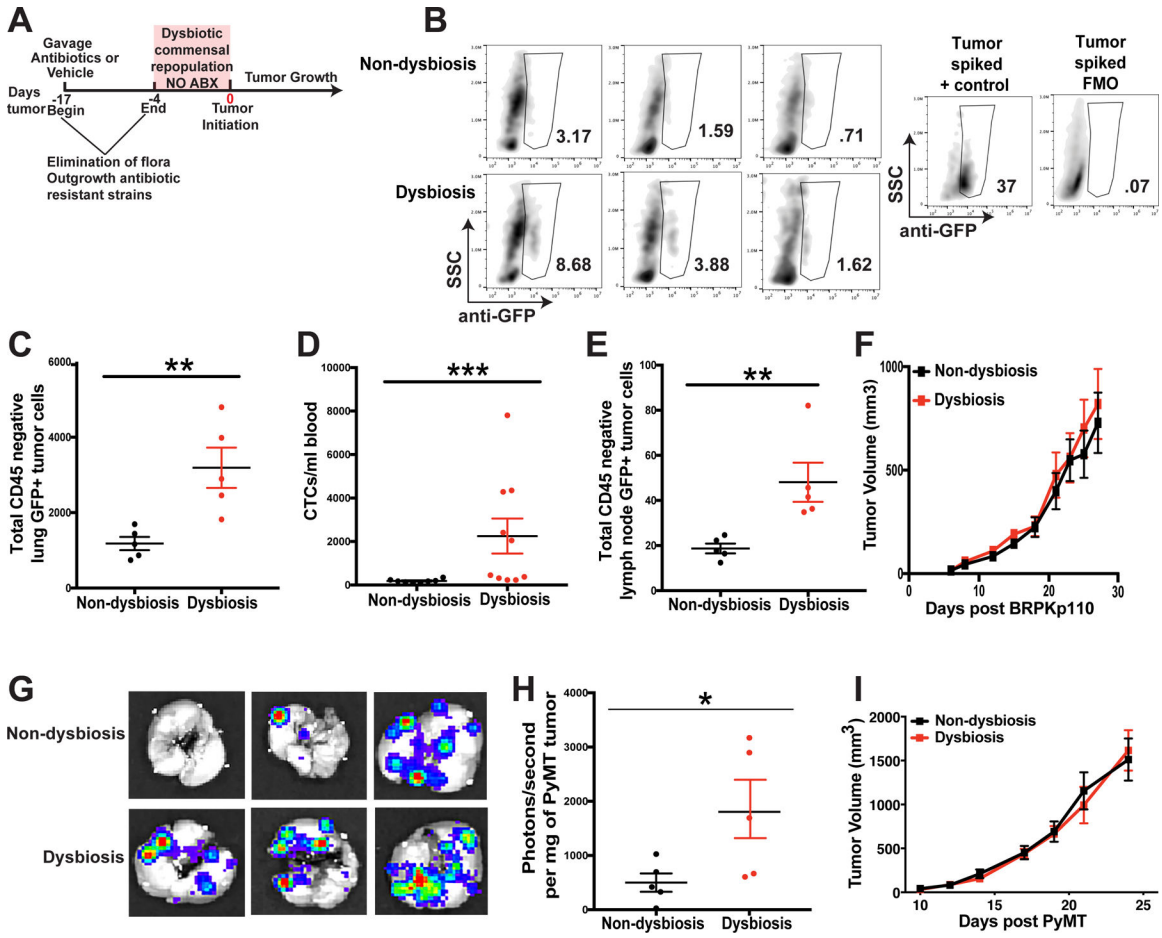

Figure 1. Commensal dysbiosis enhances mammary tumor cell dissemination.

A. Experimental design for antibiotic-induced dysbiosis and tumor initiation. C57BL/6 mice were orally gavaged for 14 days with a broad-spectrum cocktail of antibiotics or an equal volume of water as a vehicle control. Gavage was ceased four days prior to tumor initiation in the fourth mammary fat pad. Tumor size was measured by calipers every 2–3 days after reaching a palpable size. **B.** Representative plots demonstrating GFP^+ tumor cell quantitation in the lungs. The anti-GFP gate was chosen based upon fluorescence minus one (FMO) controls and a stained lung sample spiked with BRPKp110 tumor cells. Numbers represent percent cells within the anti-GFP gate of total live cells. **C-F.** C57BL/6 mice were treated as described in Fig. 1A. 27 days after BRPKp110 tumor initiation, GFP^+ tumor cell dissemination was quantified in lung tissue (**C**), peripheral blood (**D**), and tumor-draining axillary lymph nodes (**E**) by flow cytometry. Data is represented as absolute number of GFP^+CD45^- cells of live, singlet cells. **F.** Growth kinetics of BRPKp110 mammary tumors. Representative of at least three independent experiments with 5 mice/group. **G-I.** C57BL/6 mice were treated as described in Fig. 1A. 25 days after PyMT-luciferase tumor initiation, tumor cell dissemination was quantified in lung tissue by bioluminescence. **G.** Representative images of bioluminescence in lungs from advanced tumor-bearing mice bearing PyMT-luciferase tumors. **H.** Quantitation of luminescence represented as photons/second normalized to final tumor burden for mice with PyMT tumors. **I.** Growth kinetics of

PyMT mammary tumors. Representative of two independent experiments with 5 mice/group.

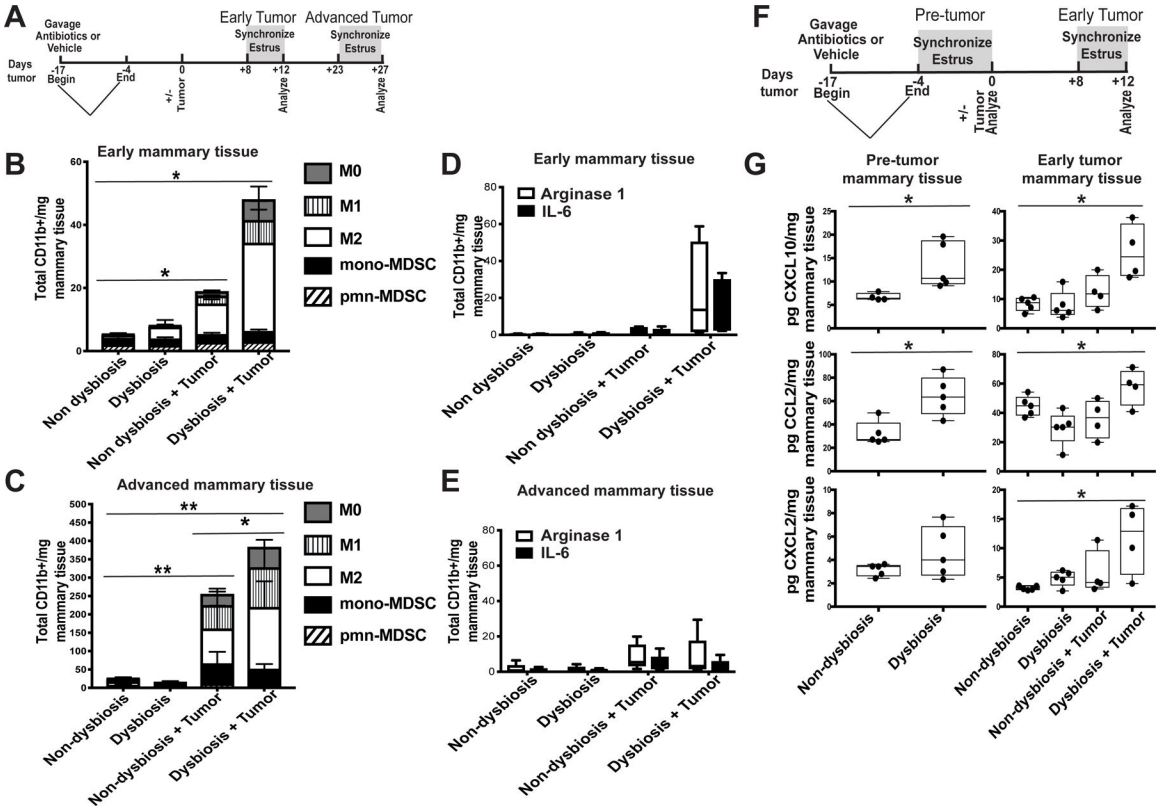

Figure 2. Dysbiosis enhances mammary gland inflammation and myeloid cell infiltration.

A. Experimental design for B-E. C57BL/6 mice were orally gavaged for 14 days with a broad-spectrum cocktail of antibiotics or an equal volume of water as a vehicle control. Gavage was ceased four days prior to BRPKp110 tumor initiation into the abdominal mammary fat pad. Mice were euthanized at early (day 12) and advanced (day 27) tumor timepoints. Four days prior to each timepoint, a modified Whitten effect was used to synchronize estrus in these animals. Normal tumor-adjacent mammary glands were harvested, and infiltrating myeloid cell populations were quantitated by flow cytometry at early (**B**) and advanced (**C**) timepoints after tumor initiation. All populations were gated on live, singlet, $CD45^{+}CD11b^{+}$ cells. Numbers represent absolute numbers of cells quantitated using counting beads. M0 macrophages = $F4/80^{+}CD86^{-}CD206^{-}$. M1 macrophages = $F4/80^{+}CD86^{+}CD206^{-}$. M2 macrophages = $F4/80^{+}CD86^{-}CD206^{+}$. Monocytic MDSC = $Ly6C^{hi}Ly6G^{-}$. Polymorphonuclear MDSC = $Ly6C^{mid}Ly6G^{+}$. Arginase-1 and IL-6 expression were quantitated by intracellular staining in bulk $CD45^{+}CD11b^{+}$ cells from mammary glands at early (**D**) and advanced (**E**) timepoints after tumor initiation. Numbers represent absolute numbers of cells quantitated using counting beads. **F.** Experimental design for G. Similar to A, C57BL/6 mice were orally gavaged for 14 days with a broad-spectrum cocktail of antibiotics or an equal volume of water as a vehicle control. Gavage was ceased four days prior to BRPKp110 tumor initiation into the abdominal mammary fat pad. Mice were euthanized prior to tumor initiation (pre-tumor; day 0) and at an early point (early tumor; day 12) during tumor progression. Four days prior to each timepoint, a modified Whitten effect was used to synchronize estrus in these animals. Normal tumor-

adjacent mammary glands were harvested, and protein levels of CXCL10, CCL2, and CXCL2 were quantitated by multiplex cytokine analysis **(G)**.

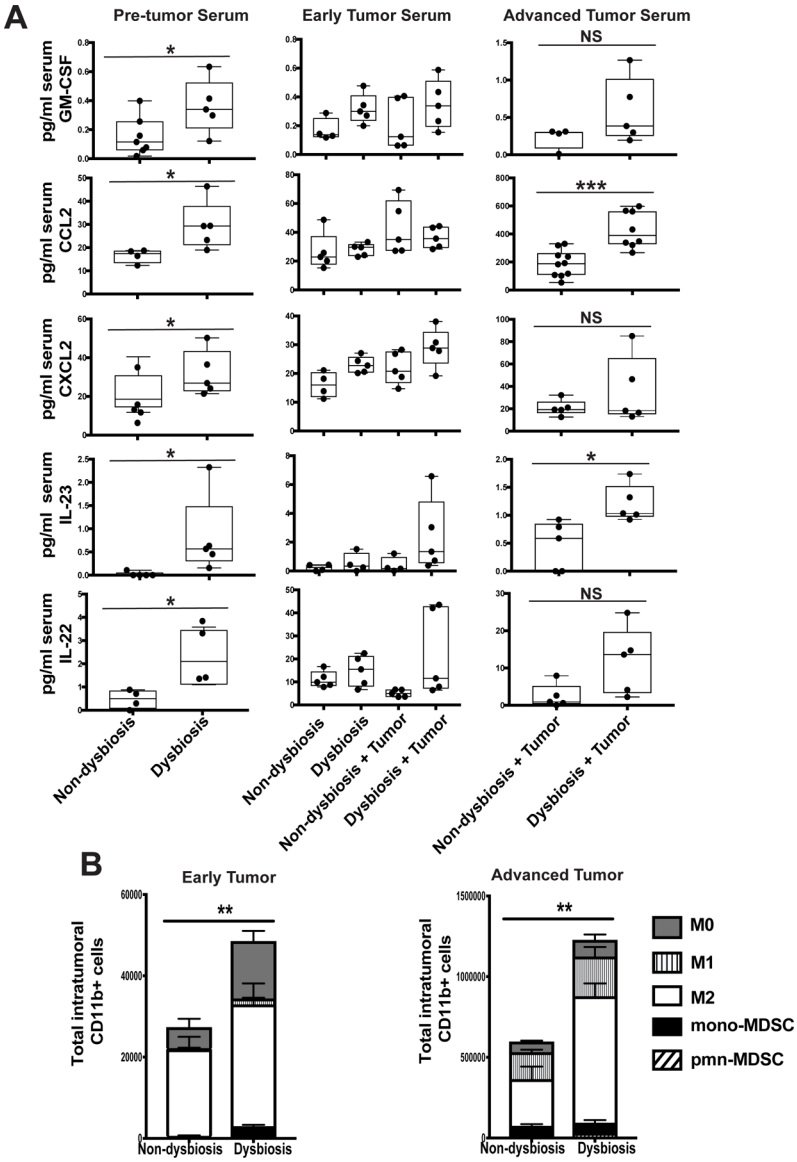

Figure 3. Dysbiosis induces early and sustained systemic inflammation and enhances myeloid infiltration into mammary tumors.

C57BL/6 mice were treated as described in Figure 2A. **A.** Serum was collected from BRPKp110 tumor- and non-tumor bearing mice, with or without established dysbiosis, at various timepoints: prior to tumor initiation (pre tumor serum; day 0), and at early (early tumor serum; day 12) and advanced (advanced tumor serum; day 27) timepoints after tumor initiation. Serum GM-CSF, CCL2, CXCL2, IL-23, and IL-22 were quantitated by multiplex cytokine analysis. **B.** BRPKp110 mammary tumors were harvested, and infiltrating myeloid cell populations were quantitated by flow cytometry at early and advanced timepoints after tumor initiation. All populations were gated on live, singlet, $CD45^{+}CD11b^{+}$ cells. Numbers represent absolute numbers of cells quantitated using counting beads. M0 macrophages = $F4/80^{+}CD86^{-}CD206^{-}$. M1 macrophages = $F4/80^{+}CD86^{+}CD206^{-}$. M2 macrophages = $F4/80^{+}CD86^{-}CD206^{+}$. Monocytic MDSC = $Ly6C^{hi}Ly6G^{-}$. Polymorphonuclear MDSC = $Ly6C^{mid}Ly6G^{+}$.

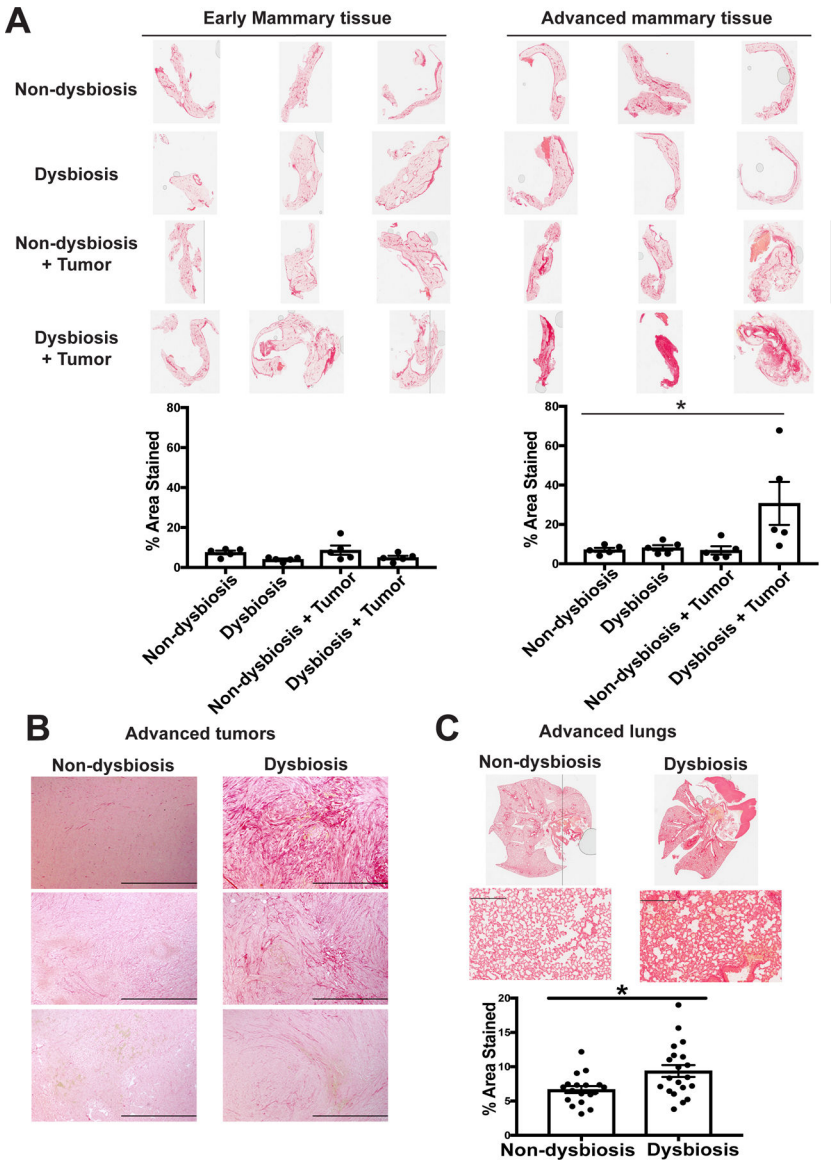

Figure 4. Dysbiosis enhances both local and systemic fibrosis within normal tumor-adjacent mammary tissue in advanced tumor-bearing animals.

C57BL/6 mice were treated as described in Figure 2A. **A.** Normal-adjacent mammary glands were harvested from BRPKp110 tumor- and non-tumor bearing mice, with or without established dysbiosis, at early (early mammary tissue; day 12) and advanced (advanced mammary tissue; day 27) timepoints after tumor initiation. BRPKp110 mammary tumors (**B**) and lungs (**C**) were harvested from advanced tumor-bearing animals with or without established dysbiosis. All tissues were formalin-fixed and paraffin-embedded, and sections were stained with PicroSirius Red. Quantification of staining intensity was calculated using Image J software.

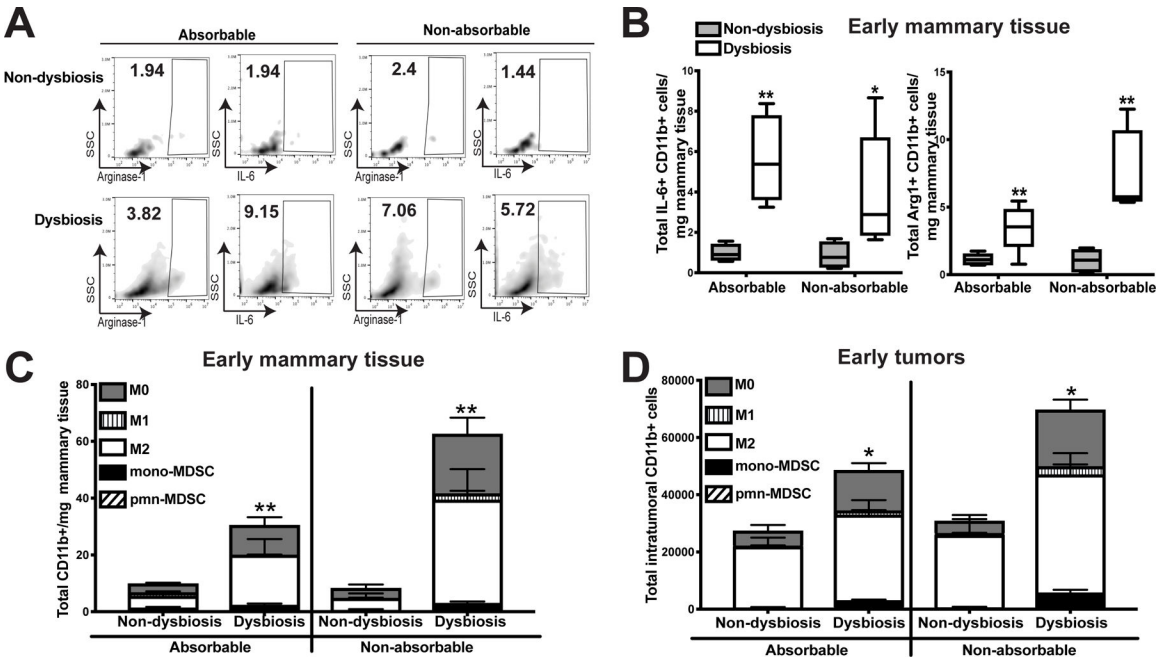

Figure 5. Direct targeting of gut commensals using non-absorbable antibiotics results in enhanced inflammation and myeloid cell infiltration in dysbiotic mice.

C57BL/6 mice were treated as described in Figure 2A. Half of the antibiotic-treated animals were gavaged with the previously-described antibiotic cocktail, while the other half were gavaged with a cocktail of non-absorbable antibiotics that have minimal absorption from the gut. Non-dysbiotic animals from each group were gavaged with similar volumes of water per the administered antibiotic cocktail. Normal tumor-adjacent mammary glands (**A-C**) and BRPKp110 tumors (**D**) were harvested at an early timepoint (12 days) after tumor initiation, and myeloid cell populations were quantitated by flow cytometry. **A**. Representative plots gating on arginase-1^{+} and IL-6^{+} myeloid cells. Numbers represent the frequency of CD11b^{+} cells positive for each factor. **B.** Arginase-1 and IL-6 expression quantitated by intracellular staining in bulk CD45^{+}CD11b^{+} cells from mammary glands. Numbers represent absolute numbers of cells quantitated using counting beads. Characterization of myeloid populations from mammary glands (**C**) or tumors (**D**). All populations were gated on live, singlet, CD45^{+}CD11b^{+} cells. Numbers represent absolute numbers of cells quantitated using counting beads. M0 macrophages = F4/80^{+}CD86^{-}CD206^{-}. M1 macrophages = F4/80^{+}CD86^{+}CD206^{-}. M2 macrophages = F4/80^{+}CD86^{-}CD206^{+}. Monocytic MDSC = Ly6C^{hi}Ly6G^{-}. Polymorphonuclear MDSC = Ly6C^{mid}Ly6G^{+}. Representative of two independent experiments with 5 mice/group

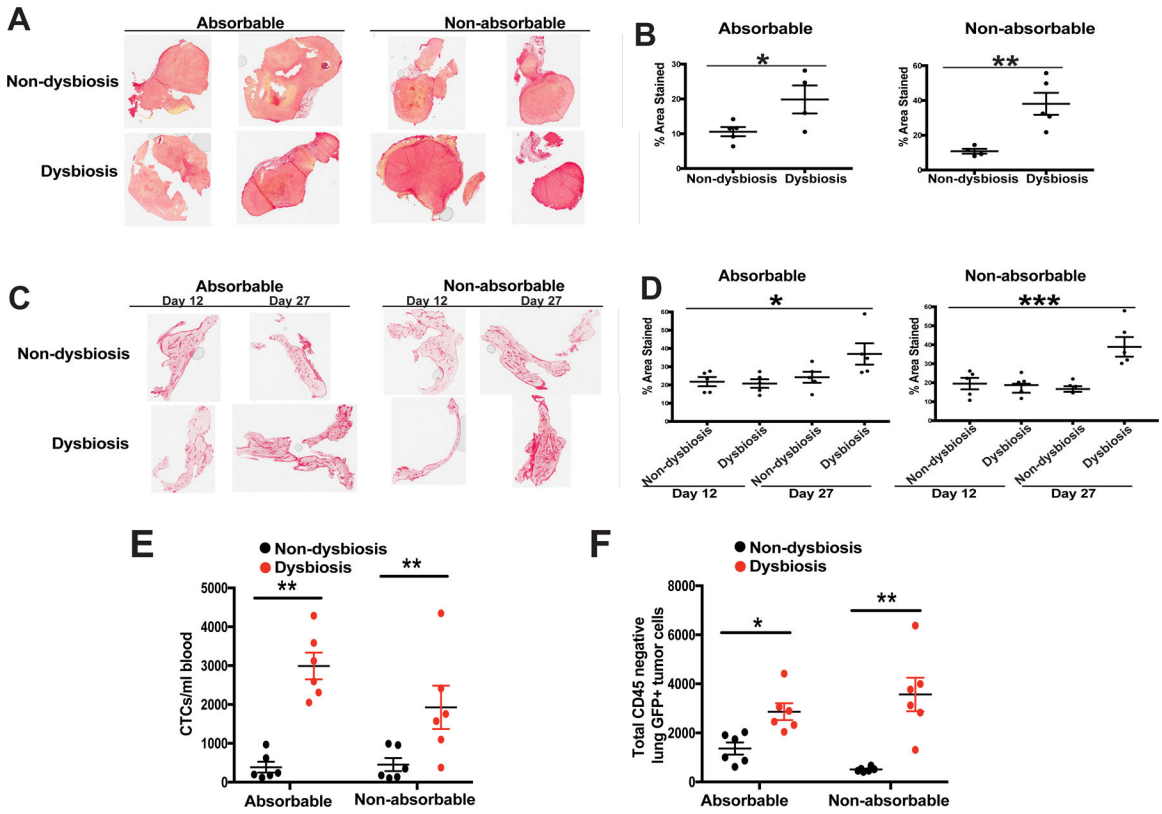

Figure 6. Direct targeting of gut commensals using non-absorbable antibiotics results in enhanced fibrosis and tumor cell dissemination in advanced tumor-bearing dysbiotic mice.

C57BL/6 mice were treated as described in Figure 2A. Half of the antibiotic-treated animals were gavaged with the previously-described antibiotic cocktail while the other half were gavaged with a cocktail of non-absorbable antibiotics that have minimal absorption from the gut. Non-dysbiotic animals from each group were gavaged with similar volumes of water per the administered antibiotic cocktail. **A.** Advanced BRPKp110 mammary tumors and **C.** normal tumor-adjacent mammary glands at early (day 12) and advanced (day 27) timepoints after tumor initiation were harvested from tumor-bearing mice, with or without established dysbiosis. Tissues were formalin-fixed and paraffin-embedded, and sections were stained with PicroSirius Red. Quantification of staining intensity was calculated using Image J software for both tumors (**B**) and mammary glands (**D**). **E-F**. GFP^+ tumor cell dissemination was quantified in peripheral blood (**E**) and lung tissue (**F**) by flow cytometry. Data is represented as absolute number of GFP^+CD45^- cells of live, singlet cells. The anti-GFP gate was chosen based upon FMOs and a stained lung sample spiked with GFP^+ BRPKp110 tumor cells. Representative of two independent experiments with 5 mice/group

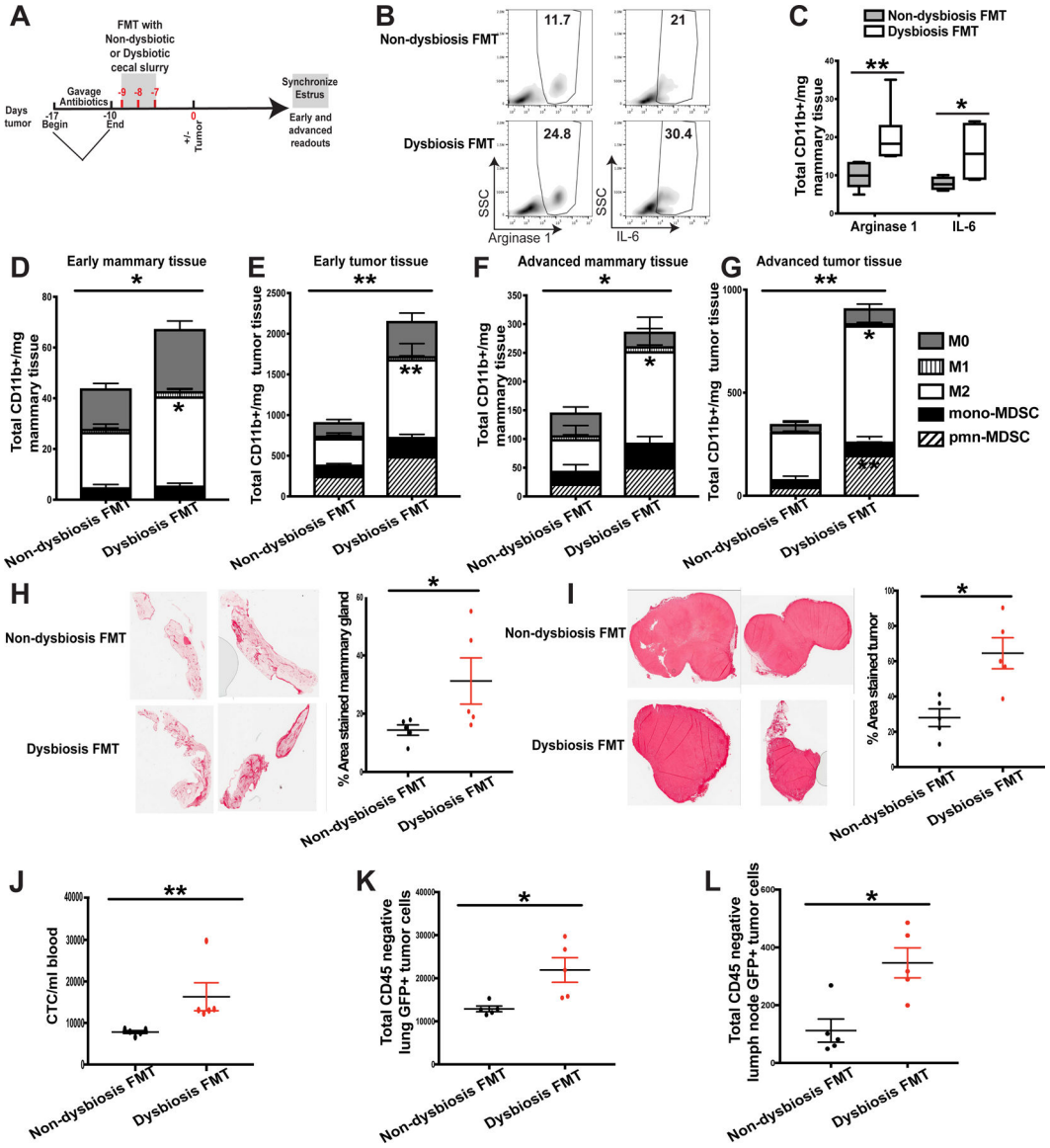

Figure 7. Fecal microbiota transplantation of dysbiotic cecal contents is sufficient to enhance inflammation, myeloid cell infiltration, fibrosis, and tumor cell dissemination.

A. Experimental design for B-L. C57BL/6 mice were orally gavaged for 7 days with a broad-spectrum cocktail of antibiotics to create a niche for fecal transplantation. Immediately following antibiotic cessation, mice received three consecutive days of oral gavage of cecal slurries collected from dysbiotic or non-dysbiotic mice from day 0, as depicted in Fig. 2A. Mice were then rested for seven days to allow for bacterial engraftment and growth prior to BRPKp110 tumor initiation into the abdominal mammary fat pad. Mice were euthanized at early (day 12) and advanced (day 27) tumor timepoints. Four days prior to each timepoint, a modified Whitten effect was used to synchronize estrus in these animals. **B-C**. Arginase-1 and IL-6 expression were quantitated by intracellular staining in bulk $CD45^{+}CD11b^{+}$ cells from mammary glands. **B.** Representative intracellular staining of arginase-1 and IL-6 from myeloid cells within normal-adjacent mammary glands. Numbers represent percent of total $CD11b^{+}$ myeloid cells. **C.** Quantitation of $CD11b^{+}$ cells producing

arginase-1 or IL-6. Numbers represent absolute numbers quantitated using counting beads. **D-G**. Mammary glands and tumors were harvested at early or advanced tumor timepoints and myeloid cell populations were quantitated by flow cytometry. All populations were gated on live, singlet, $CD45^{+}CD11b^{+}$ cells. Numbers represent absolute numbers of cells quantitated using counting beads. **D.** Absolute number of myeloid populations in early mammary glands. **E.** Absolute number of myeloid populations in early tumors. **F.** Absolute number of myeloid populations in advanced mammary glands. **G.** Absolute number of myeloid populations in advanced tumors. M0 macrophages = $F4/80^{+}CD86^{-}CD206^{-}$. M1 macrophages = $F4/80^{+}CD86^{+}CD206^{-}$. M2 macrophages = $F4/80^{+}CD86^{-}CD206^{+}$. Monocytic MDSC = $Ly6C^{hi}Ly6G^{-}$. Polymorphonuclear MDSC = $Ly6C^{mid}Ly6G^{+}$. Normal-adjacent mammary glands (**H**) and tumors (**I**) were harvested from advanced tumor-bearing animals that received either dysbiotic or non-dysbiotic FMT. Tissues were formalin-fixed and paraffin-embedded, and sections were stained with PicroSirius Red. Quantification of staining intensity was calculated using Image J software. Representative of two independent experiments with 5 mice/group. **J-L**. GFP^{+} tumor cell dissemination was quantified in peripheral blood (**J**) lung tissue (**K**) and distal axillary lymph nodes (**L**) by flow cytometry. Data is represented as absolute number of $GFP^{+}CD45^{-}$ cells of live, singlet cells. The anti-GFP gate was chosen based upon FMOs and a stained lung sample spiked with GFP^{+} BRPKp110 tumor cells. Representative of two independent experiments with 5 mice/group.